

Causal Reversal in the $M_{\bullet}-\sigma_0$ Relation: Implications for High-Redshift Supermassive Black Hole Mass Estimates

BENJAMIN L. DAVIS ,¹ SAAKSHI MORE,¹ ZEHAO JIN (金泽灏) ,^{2,1} MARIO PASQUATO ,³ ANDREA VALERIO MACCIÒ ,¹
AND FENG YUAN (袁峰) 

¹Center for Astrophysics and Space Science (CASS), New York University Abu Dhabi, PO Box 129188, Abu Dhabi, UAE

²Center for Astronomy and Astrophysics and Department of Physics, Fudan University, Shanghai 200438, People's Republic of China

³Istituto Nazionale di Astrofisica, IASF-Milano Via Alfonso Corti 12, I-20133 Milano, Italy

(Received November 10, 2025)

Submitted to AAS Journals

ABSTRACT

The nascent methodology of applying the principles of causal discovery to astrophysical data has produced affirming results about deeply held theories concerning the causal nature behind the observed coevolution of supermassive black holes (SMBHs) with their host galaxies. The key results from observations have demonstrated an apparent causal reversal across different galaxy morphologies—SMBHs causally influence the evolution of the physical parameters of their spiral galaxy hosts, whereas SMBHs in elliptical galaxies are passive companions that grow in near lockstep with their hosts. To further explore and ascertain insights, it is necessary to utilize galaxy simulations to track the time evolution of the observed causal relations to learn more about the temporal nature of the changing SMBH/galaxy evolutionary directions. We conducted experiments with the NIHAO suite of cosmological zoom-in hydrodynamical simulations to follow the evolution of individual galaxies along with their central SMBH masses (M_{\bullet}) and properties including central stellar velocity dispersion (σ_0). We reproduce the causal results from real galaxies, but add clarity by observing the SMBH/galaxy causal directions are noticeably inverted between the epochs before and after the peak of star formation. The implications for causal reversal of the $M_{\bullet}-\sigma_0$ relation portend larger concerns about the reliability of SMBH masses estimated at high redshifts and presumptions of overmassive black holes at early epochs. Toward this problem, we apply updated causally-informed scaling relations that predict high- z black hole masses that are approximately two orders of magnitude less massive, and thus not overmassive with respect to local $z = 0$ SMBH–galaxy mass ratios.

Keywords: Black hole physics (159); Galaxies (573); Galaxy dynamics (591); Galaxy evolution (594); Galaxy kinematics (602); Galaxy nuclei (609); Galaxy physics (612); Galaxy properties (615); Hydrodynamical simulations (767); Supermassive black holes (1663)

1. INTRODUCTION

It is widely believed that some fraction of the bolometric luminosity of an accreting supermassive black hole (SMBH) couples thermally with the surrounding gas in its host galaxy. This energy deposition suggests a feedback mechanism that may regulate the growth of an SMBH by expelling gas from its host galaxy and quenching star formation (A. Mastichiadis & J. G. Kirk 1995;

L. Ciotti & J. P. Ostriker 1997; L. Ciotti & T. S. van Albada 2001; J. Silk & M. J. Rees 1998; S. Ikeuchi 1999; A. Renzini 2000; J. S. B. Wyithe & A. Loeb 2003). Indeed, V. Springel et al. (2005) presented hydrodynamical simulations of galaxy mergers, showing how active galactic nuclei (AGNs) feedback regulates star formation and SMBH growth. The feedback quenches star formation, leading to the formation of red elliptical galaxies, providing a compelling explanation for the observed galaxy color bimodality. This feedback mechanism suggests a mechanism whereby an SMBH may causally af-

fect its much larger host galaxy, which is typically between $\approx 10^2$ – 10^4 times more massive at $z = 0$ (N. Sahu et al. 2019a, their Fig. 12).

The early theoretical and observational groundwork for AGN feedback was laid three decades ago, and numerical simulations for the past two decades have demonstrated a clear dependency on including the feedback prescriptions in their models in order to reproduce the observed population of red elliptical galaxies in the local Universe. Along the way, some observational evidence has been presented to support the notion of AGN feedback (e.g., K. Schawinski et al. 2007; A. C. Fabian 2012; R. Morganti 2017; C. M. Harrison & C. Ramos Almeida 2024). Of course, one of the most notable connections between galaxy formation and SMBHs is the correlation seen between the stellar velocity dispersion of bulges and the masses of SMBHs they host (e.g., L. Ferrarese & D. Merritt 2000; K. Gebhardt et al. 2000; S. Tremaine et al. 2002; J. Kormendy & L. C. Ho 2013; N. Sahu et al. 2019b). However, despite the extensive foundation for AGN feedback established by theory/simulations and supportive correlations uncovered from observational searches, there had not been a conclusive affirmation of a causal relation (i.e., a clear cause/effect relationship beyond a superficial correlation), nor its direction (i.e., which observable is a cause and which is an effect). Recently, studies have sought to bring causal discovery (J. Pearl 2000; A. Zanga et al. 2023; M. Huber 2024) techniques to this problem (M. Pasquato et al. 2023; M. Pasquato 2024; Z. Jin et al. 2024, 2025b,c).

We studied a sample of 101 SMBHs with dynamically-measured masses in our previous work by Z. Jin et al. (2025c), hereafter Paper I. In addition to SMBH mass (M_\bullet), their sample also included six measurements of the 101 host galaxies, divided into 35 elliptical, 38 lenticular, and 28 spiral galaxies. These galaxy measurements included the central stellar velocity dispersion (σ_0), effective (half-light) radius of the bulge (R_e), the average projected density within R_e ($\langle \Sigma_e \rangle$), total stellar mass of the entire galaxy (M^*), color (W2–W3), and specific star formation rate (sSFR). These chosen galaxy parameters provide a nice manifold from which to test the causal relationships between the SMBH mass. While our observational study was not afforded with time series data of the galaxies, the separation of galaxies into their morphologies allowed for a progressive evolutionary study of causal directions from young spiral galaxies to old elliptical galaxies. In our present study, we repeat the methodology of Paper I, but with simulations to directly track the causal structures with time.

Paper I performed an exhaustive Bayesian analysis of all 1,138,779,265 possible directed acyclic graphs (DAGs) for the possible permutations of their M_\bullet plus six galaxy parameters for morphologically-distinct samples.⁴ Among the score-based causal directions uncovered between all variables, perhaps the most revealing result concerns the morphologically-dependent causal directions uncovered in the M_\bullet – σ_0 relation. Paper I found that in *spiral galaxies*, $\sigma_0 \rightarrow M_\bullet$ (i.e., σ_0 directly causes M_\bullet , such that σ_0 is considered a parent of M_\bullet) 22% of the time. Conversely for *elliptical galaxies*, $\sigma_0 \rightarrow M_\bullet$ in 78% of all cases. Unsurprisingly, lenticulars lie somewhere in the middle, with $\sigma_0 \rightarrow M_\bullet$ satisfying 72% of all scenarios.

In *elliptical galaxies*, σ_0 is the causal driver of change (i.e., growth) in M_\bullet . Whereas, σ_0 is not the driver of change in M_\bullet in spiral galaxies, therefore it is more likely that M_\bullet drives the change in σ_0 . Paper I concluded that this naturally implies that an SMBH is able to affect change in its host spiral galaxy, likely through AGN feedback. Given the rich supplies of gas typically available in spiral galaxies, this allows a causal pathway for an active SMBH to progressively quench its host galaxy. By the time a host galaxy has evolved into an elliptical galaxy, the quenching process is complete and the gas supply has been largely exhausted, leaving no medium for an SMBH to continue causally affecting its host galaxy. This transition places an SMBH as a passive passenger in its host elliptical galaxy, leaving it to only evolve as its host causally allows through accretion and mergers.

The novel work of Paper I offered a unique observational confirmation of AGNs feedback and cements SMBHs and their host galaxies together via their shared coevolution. In the present study, we endeavor to advance the study of Paper I into the temporal domain by tracking the time series changes in causal directions between SMBHs and their host galaxies via hydrodynamical simulations. In particular, our simulations include prescriptions of AGNs feedback. Thus, the efforts of this work will aim to strengthen the observational confirmation of AGNs feedback presented in Paper I. Over the course of this paper, we present our methodology of using numerical simulations (§2), exhibit our results (§3), derive new causally-informed scaling relations (§4), and provide a discussion of our findings, their implications, and overall importance (§5). Throughout this work, all mean values are quoted with ± 1 standard deviation un-

⁴ We look up the number of DAGs with n labeled nodes from The On-Line Encyclopedia of Integer Sequences (<https://oeis.org/A003024>).

certainties and all median values are quoted with ± 1 median absolute deviation uncertainties.

2. NUMERICAL SIMULATIONS

We conduct our study using simulated galaxies from the NIHAO (Numerical Investigation of a Hundred Astrophysical Objects) Project (L. Wang et al. 2015; M. Blank et al. 2019), which are cosmological zoom-in hydrodynamical simulations performed using the `Gasoline2` code (J. W. Wadsley et al. 2017) with an improved smoothed particle hydrodynamics algorithm. NIHAO simulations are designed to study galaxy formation and evolution, covering a broad range of dark matter halo masses, from dwarf galaxies to massive ellipticals. The primary goal of the project is to realistically model the complex processes involved in how galaxies form stars, grow, and change over cosmic time. NIHAO simulations have been very successful in reproducing observed relationships, such as the inefficiency of galaxy formation (the stellar mass to halo mass relation) and the connection between star formation rates and stellar masses (M. Blank et al. 2019). A key focus is understanding the impact of stellar feedback and the influence of SMBHs on their host galaxies. By comparing these detailed simulations with observational data, the NIHAO project provides crucial insights into the physical mechanisms that drive galaxy evolution and shape the properties of galaxies, including their dark matter halos, across the Universe.

2.1. Galaxy Property Extraction

For each central galaxy in our NIHAO sample, we extract five physical properties for causal discovery analysis, measured at every simulation snapshot with the `pynbody` package (A. Pontzen et al. 2013):

- **Black hole mass (M_{\bullet}):** Mass of the *most massive black hole particle* in the central halo, isolating the primary SMBH and excluding lower-mass merger remnants. Reported in solar units using the `pynbody` particle filter and halo catalog.
- **Stellar mass (M^*):** Total mass of all bound star particles in the central halo, converted to solar mass units.
- **Effective radius (R_e):** Three-dimensional spherical half-light radius. Defined as the radius enclosing half of the total V -band luminosity of the stellar population, reported in kiloparsecs.
- **Central velocity dispersion (σ_0):** Stellar velocity dispersion of bulge stars within 5 kpc and

with negative angular momentum (random, non-rotational motion) along the z -axis ($j_z < 0$). A logarithmic radial profile (100 bins) is constructed, and the dispersion is interpolated within 595 pc.⁵

- **Specific star formation rate (sSFR):** Ratio of the star formation rate (SFR) to total stellar mass. The SFR is obtained by binning the star formation history into the 64 simulation snapshots (216 Myr spacing). The resulting sSFR, in units of Gyr^{-1} , quantifies star formation activity relative to stellar mass.

3. RESULTS

3.1. Star-forming and Quenched Galaxies

We begin our study by looking at 55 simulated galaxies that reached $z = 0$ and grouping them into 28 star-forming galaxies and 27 quenched galaxies. We classify the galaxies as either star-forming or quenched at $z = 0$ by a cut in the SFR at $\log(\text{sSFR}/\text{yr}^{-1}) = -11$ (see the *left* plot in Figure 1). This cut is such that it produces a clear bimodal distribution across all of the galaxy parameters (see the *right* plot in Figure 1). Coincidentally, this sSFR cut also divides our sample almost in half (28 vs. 27).

Over the evolution of our simulated galaxies, we track the SFR of our galaxies as a function of time (Figure 2). At $z = 0$, some galaxies have not yet reached their peak SFR; these galaxies are still in their “star-forming” phases. Conversely, other galaxies at $z = 0$ have already reached their peak SFR and are now on the decline (Figure 2); these galaxies have reached their “quenched” phase. This turnover in the star-formation rate helps us distinguish between a galaxy’s period of active star formation and its subsequent period of quenching, where star formation slows or stops.

3.2. Confirmation of a Causal Reversal

Having grouped our simulated galaxies into star-forming and quenched, we then perform our causal discovery by computing the score-based exact posterior Bayesian distribution (see Paper I, for complete details) for all 29,281 unique DAGs for our combination of five simulated parameters (M_{\bullet} , σ_0 , R_e , M^* , and sSFR). We present the sum contributions from all DAGs in edge and path marginal⁶ matrices along with the corresponding

⁵ Chosen to match the homogenized dispersions of I. Jorgensen et al. (1995) in HyperLEDA (D. Makarov et al. 2014) and the observational analysis of Paper I.

⁶ The terminology *edge* and *path* marginals refer to the type of connections in a DAG. Edge marginals refer to all direct

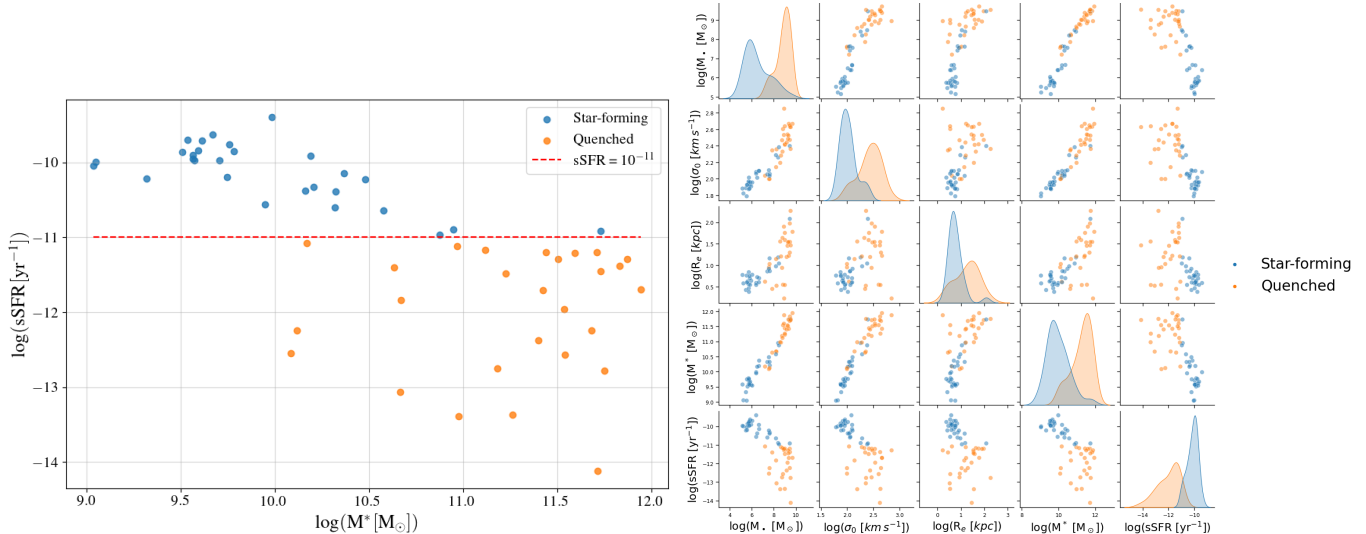


Figure 1. *Left:* A plot of specific star-formation rate vs. stellar mass. Here, we use a cut (.....) at $\log(\text{sSFR}/\text{yr}^{-1}) = -11$ to demarcate the 28 star-forming galaxies (●) from the 27 quenched galaxies (○). *Right:* A pairplot of all the investigated parameters for the galaxies in this study. This pairplot illustrates the effectiveness of the $\log(\text{sSFR}/\text{yr}^{-1}) = -11$ cut, which creates a clear bimodal distribution across all of the variables between star-forming galaxies and quenched galaxies.

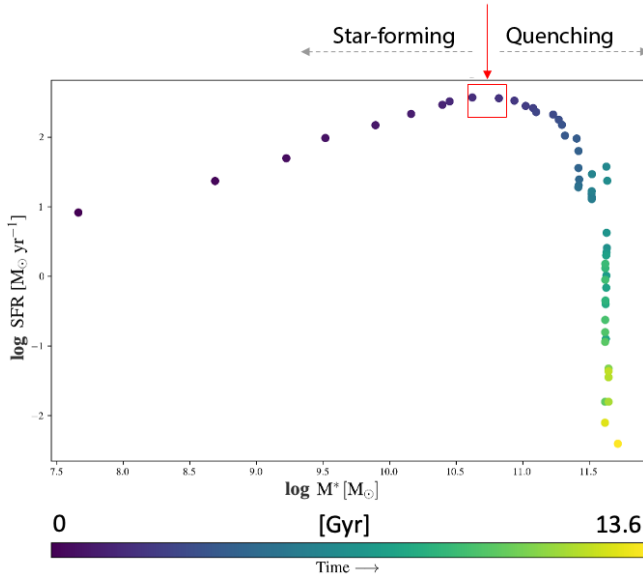


Figure 2. Evolution of a typical NIHAO galaxy that transitions from star-forming to quenching (one of 27). The plot shows the star-formation rate as a function of stellar mass. The stellar mass increases approximately monotonically as a function of time (indicated by the color of the marker). The star-formation rate initially increases until it reaches a maximum and then it steadily decreases. We use this turnover in the star-formation rate as a discriminator between a galaxy's star-forming epoch and its quenching epoch.

connections (i.e., an arrow directly from one node to another), while path marginals refer to all direct and indirect connections between nodes. For this reason, the variables in edge marginals are referred to as “parent/child” versus “ancestor/descendant” in path marginals. Thus, path marginal values are always

single most probable DAG in Figure 3. Focusing primarily on the parent/child relationships with M_\bullet , we find a clear trend of M_\bullet being a *parent* of all galaxy properties in star-forming galaxies, and oppositely a *child* of all galaxy properties in quenched galaxies.⁷ These results are in tight agreement with the morphologically-separated (spiral galaxies vs. elliptical galaxies, respectively) samples in the observational study of Paper I.

In Table 1, we provide a comparison of all our edge and path marginals for simulated and the corresponding results for observed galaxies from Paper I. In each case, we group together and compare the values for *spiral* galaxies from the observational study of Paper I with *star-forming* galaxies from our simulation study. Similarly, we group together and compare the values for *elliptical* galaxies from the observational study of Paper I with *quenched* galaxies from our simulation study. Overall, we find close agreement in the causal directions and relative edge and path marginal values between the observed and simulated galaxies.

In particular, we focus on the edge marginals concerning the $M_\bullet-\sigma_0$ relation, i.e., $P(M_\bullet \rightarrow \sigma_0)$ and $P(\sigma_0 \rightarrow M_\bullet)$. We find $P(M_\bullet \rightarrow \sigma_0) = 62\%$ for *observed* spiral galaxies vs. 58% for *simulated* star-forming

greater than or equal to edge marginal values because parents are always ancestors of their children, but ancestors are not always parents of their descendants.

⁷ To clarify, we find that SMBHs are not significantly causing galaxy properties in quenched galaxies, *as long as the galaxy remains quenched*. The caveat here is that if star formation gets reignited in a galaxy, this will allow the SMBH to reestablish causal influence on its host galaxy via AGN feedback.

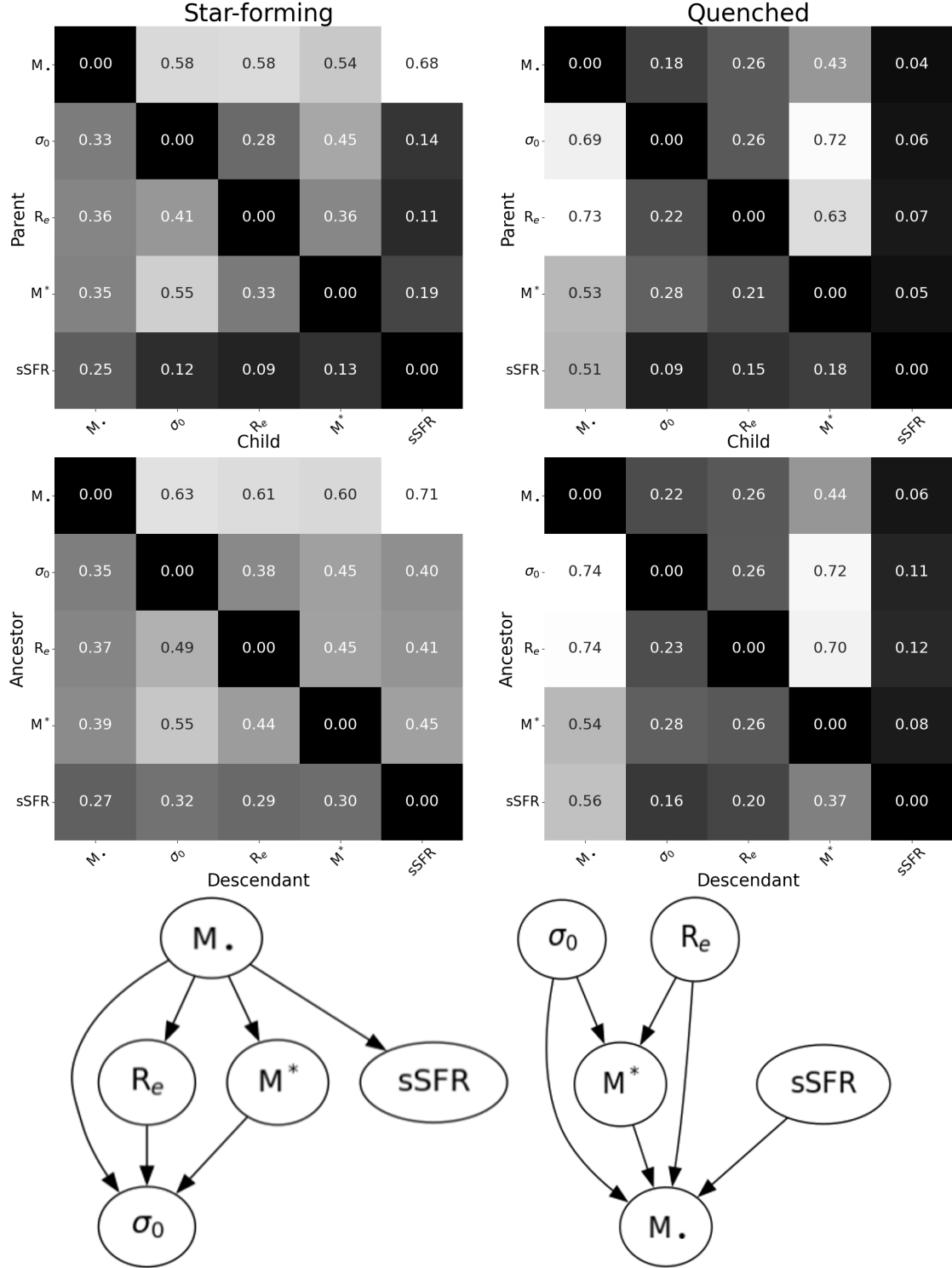


Figure 3. Edge (top row) and path (middle row) marginal matrices and the most probable directed acyclic graphs (DAGs; bottom row) for the 28 simulated star-forming galaxies (left column) and 27 simulated quenched galaxies (right column) at $z = 0$. These matrices clearly indicate a change in color between the first rows of each matrix and also between the first columns of each matrix. These changes represent higher probabilities for M_\bullet causing host galaxy properties for star-forming galaxies (left matrices) and M_\bullet being caused by properties of their host galaxies in quenched galaxies (right matrices). Indeed, the corresponding DAGs reflect M_\bullet directly or indirectly causing all the simulated properties of its host galaxy in star-forming galaxies (left DAG) and M_\bullet being caused by all simulated properties of its host galaxy in quenched galaxies (right DAG).

Table 1. Comparison Between Observed and Simulated Galaxies at $z = 0$

Parent	M_{\bullet}	Child			M^*	ssSFR
		σ_0	R_e	M^*		
M_{\bullet}	...	(0.62, 0.58), (0.19, 0.18)	(0.51, 0.58), (0.30, 0.26)	(0.69, 0.54), (0.22, 0.43)	(0.35, 0.68), (0.08, 0.04)	
σ_0	(0.22, 0.33), (0.78, 0.69)	...	(0.10, 0.28), (0.59, 0.26)	(0.11, 0.45), (0.52, 0.72)	(0.23, 0.14), (0.07, 0.06)	
R_e	(0.25, 0.36), (0.15, 0.73)	(0.10, 0.41), (0.17, 0.22)	...	(0.09, 0.36), (0.46, 0.63)	(0.13, 0.11), (0.05, 0.07)	
M^*	(0.30, 0.35), (0.49, 0.53)	(0.18, 0.55), (0.22, 0.28)	(0.17, 0.33), (0.54, 0.21)	...	(0.50, 0.19), (0.05, 0.05)	
ssSFR	(0.13, 0.25), (0.76, 0.51)	(0.17, 0.12), (0.11, 0.09)	(0.06, 0.09), (0.16, 0.15)	(0.20, 0.13), (0.13, 0.18)	...	
Descendant						
Ancestor	M_{\bullet}	σ_0	R_e	M^*		ssSFR
M_{\bullet}	...	(0.71, 0.63), (0.20, 0.22)	(0.63, 0.61), (0.43, 0.26)	(0.69, 0.60), (0.37, 0.44)	(0.74, 0.71), (0.09, 0.06)	
σ_0	(0.25, 0.35), (0.79, 0.74)	...	(0.30, 0.38), (0.76, 0.26)	(0.30, 0.45), (0.72, 0.72)	(0.41, 0.40), (0.16, 0.11)	
R_e	(0.30, 0.37), (0.38, 0.74)	(0.36, 0.49), (0.20, 0.23)	...	(0.33, 0.45), (0.46, 0.70)	(0.40, 0.41), (0.09, 0.12)	
M^*	(0.31, 0.39), (0.56, 0.54)	(0.31, 0.55), (0.27, 0.28)	(0.37, 0.44), (0.54, 0.26)	...	(0.59, 0.45), (0.11, 0.08)	
ssSFR	(0.22, 0.27), (0.80, 0.56)	(0.37, 0.32), (0.23, 0.16)	(0.32, 0.29), (0.57, 0.20)	(0.35, 0.30), (0.51, 0.37)	...	

NOTE— Edge (*top*) and path (*bottom*) marginal values. The nested ordered pairs indicate the following: (*observed* spiral galaxies, *simulated* star-forming galaxies), (*observed* elliptical galaxies, *simulated* quenched galaxies). Consider the parent/child relationship above: $P(M_{\bullet} \rightarrow \sigma_0) = (0.62, 0.58), (0.19, 0.18)$. The first nested ordered pair demonstrates the probability that M_{\bullet} is a parent of σ_0 in *observed* spiral galaxies is 62% vs. 58% for *simulated* star-forming galaxies. The second nested ordered pair demonstrates the probability that M_{\bullet} is a parent of σ_0 in *observed* elliptical galaxies is 19% vs. 18% for *simulated* star-forming galaxies. Therefore, these comparisons show a tight agreement between observed and simulated galaxies, in the case of $P(M_{\bullet} \rightarrow \sigma_0)$. All simulated values are obtained from our Fig. 3, while all observed values are imported from Paper I, their Fig. 4.

galaxies. Similarly, we find $P(M_{\bullet} \rightarrow \sigma_0) = 19\%$ for *observed* elliptical galaxies vs. 18% for *simulated* quenched galaxies. For the opposite causal direction $P(\sigma_0 \rightarrow M_{\bullet})$, we find 22% for *observed* spiral galaxies vs. 33% for *simulated* star-forming galaxies. Similarly, we find $P(\sigma_0 \rightarrow M_{\bullet}) = 78\%$ for *observed* elliptical galaxies vs. 69% for *simulated* quenched galaxies.⁸ These comparisons demonstrate a dominant preferential causal direction from $M_{\bullet} \rightarrow \sigma_0$ for both *observed* spiral galaxies and *simulated* star-forming galaxies. Complementarily, we find a dominant preferential causal direction from $\sigma_0 \rightarrow M_{\bullet}$ for both *observed* elliptical galaxies and *simulated* quenched galaxies.

3.3. Causal Reversal in the $M_{\bullet}-\sigma_0$ Relation

In Figure 4, we present a graphical representation of the time evolution of the causal $M_{\bullet}-\sigma_0$ relation, relative to a galaxy’s age at the peak of star-formation (T_{peak}) and at $z = 0$ ($T_{z=0}$). This timeline of causality demonstrates how $P(M_{\bullet} \rightarrow \sigma_0) > P(M_{\bullet} \leftarrow \sigma_0)$ is consistent from snapshots $T_{\text{peak}} - 1079$ Myr to $T_{\text{peak}} - 432$ Myr. The snapshots at T_{peak} , and closest to the peak of star formation (from $T_{\text{peak}} - 216$ Myr to $T_{z=0} - 863$ Myr), show a period of transition where $P(M_{\bullet} \rightarrow \sigma_0) > P(M_{\bullet} \leftarrow \sigma_0)$ switches to $P(M_{\bullet} \rightarrow \sigma_0) < P(M_{\bullet} \leftarrow \sigma_0)$, and back again. This period of transition could be analogous to the variability in a galaxy as its black hole grows and it moves toward quiescence, as exhibited by its fluctuating fraction of cool gas (T. Wang et al. 2024). Following the transition, the snapshots settle to $P(M_{\bullet} \rightarrow \sigma_0) < P(M_{\bullet} \leftarrow \sigma_0)$ from snapshots $T_{z=0} - 647$ Myr to $T_{z=0}$. Therefore, we consider our simulated galaxies to firmly have the $M_{\bullet} \rightarrow \sigma_0$ causal direction during their evolution *up to* 432 Myr before their peak star-formation rate, and decidedly flip to $M_{\bullet} \leftarrow \sigma_0$ for their futures *beyond* 647 Myr before $T_{z=0}$. This temporal evolution of the $M_{\bullet}-\sigma_0$ relation provides a more finely resolved nature of the causal reversal discovered by Paper I from analyzing observations of real galaxies segregated by morphology.

⁸ The opposing causal directions of the marginals do not necessarily add up to one, i.e., $P(X \rightarrow Y) + P(X \leftarrow Y) \leq 1$. This is because there may be some probability that X and Y are disconnected. Counterintuitively, the edge marginals for the null case (i.e., the posterior from a uniform prior without any data) *do not* imply equal probabilities (i.e., 1/3) for $X \rightarrow Y$, $X \leftarrow Y$, and $X \perp\!\!\!\perp Y$ (X and Y are independent). Although, $P(X \rightarrow Y) = P(X \leftarrow Y)$ must be satisfied in the null case. The *edge* marginals for the null case without any data for five variables is $P(X \rightarrow Y) = P(X \leftarrow Y) = 30\%$ and $P(X \rightarrow Y) = P(X \leftarrow Y) = 40\%$ for *path* marginals.

4. CAUSALLY-INFORMED SCALING RELATIONS

We use the linear regression software Hyper-Fit (A. S. G. Robotham & D. Obreschkow 2015, 2016) to accurately fit our relations from the observational data of Paper I while fully considering uncertainties in all variables and intrinsic scatter. Since we will be working entirely in logarithmic space, we make the following notations for simplicity: $\mathcal{M}_{\bullet} \equiv \log(M_{\bullet}/M_{\odot})$ and $\mathcal{S}_0 \equiv \log(\sigma_0/\text{km s}^{-1})$. We will consider \mathcal{M}_{\bullet} to be the black hole mass derived from the causal $M_{\bullet} \leftarrow \sigma_0$ direction. Conversely, we will represent the anti-causal ($M_{\bullet} \rightarrow \sigma_0$) as \mathcal{M}'_{\bullet} . We will denote the intrinsic scatter on the dependent variable in all relations as ϵ , which *is already included* in our relations. We note that the $M_{\bullet}-M^*$ relation also demonstrates an equivalent causal reversal (see Fig. 3). Because the $M_{\bullet}-M^*$ relation is also useful for predicting black hole masses at high- z , we will also similarly present its relations here with $\mathcal{M}^* \equiv \log(M^*/M_{\odot})$.

4.1. Baseline: All Galaxies

Most $M_{\bullet}-\sigma_0$ relations in the literature are fit to varied samples of all galaxy types grouped together in heterogeneous mixes of morphological types. However, as we have demonstrated with our causal analysis, this is not appropriate due to the mixing of the causal and anti-causal directions from quenched and star-forming galaxies, respectively. For comparison purposes, we fit the “wrong” (\mathcal{M}'_{\bullet}) black hole mass as a function of central stellar velocity dispersion from the sample of 101 galaxies (spirals, lenticulars, and ellipticals) from Paper I.

$$\mathcal{M}'_{\bullet} = (8.25 \pm 0.46) + (4.92 \pm 0.02)(\mathcal{S}_0 - 2.28) \quad (1)$$

$$\epsilon = 0.46 \pm 0.04$$

Similarly, we also fit the wrong black hole mass as a function of stellar mass.

$$\mathcal{M}'_{\bullet} = (8.01 \pm 0.66) + (1.52 \pm 0.01)(\mathcal{M}^* - 10.63) \quad (2)$$

$$\epsilon = 0.66 \pm 0.05$$

4.2. Spiral (i.e., Star-forming) Galaxies

For the “correct” causal direction for star-forming galaxies, we consider the sample of 28 spiral galaxies from Paper I and fit σ_0 as a function of M_{\bullet} , and then invert the relation.

$$\mathcal{S}_0 = (2.12 \pm 0.08) + (0.12 \pm 0.01)(\mathcal{M}_{\bullet} - 7.07)$$

$$\epsilon = 0.08 \pm 0.02$$

$$\mathcal{M}_{\bullet} = 7.07 + \frac{\mathcal{S}_0 - (2.12 \pm 0.08)}{0.12 \pm 0.01} \quad (3)$$

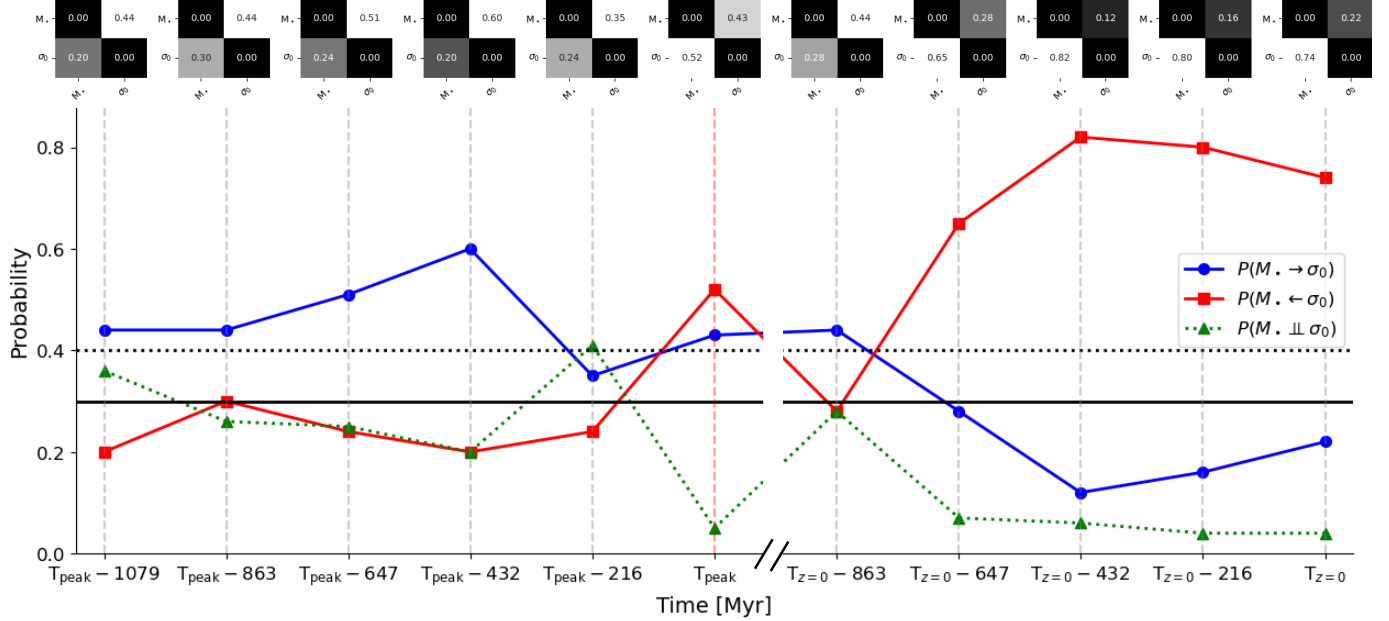


Figure 4. Time evolution of the causal M_{\bullet} - σ_0 relation. Here, we reduce the full 5×5 edge marginal matrices to only the 2×2 matrices concerning SMBH mass and central stellar velocity dispersion for our simulated galaxies, with 27 galaxies in our sample completing their evolution from star-forming to quenched by $z = 0$. These marginal matrices are listed across the top of the plot, with x -axes depicting causal children and the y -axes depicting causal parents. We select eleven matrices from successive snapshots, centered at the peak of star formation at T_{peak} (the vertical $\dashdot\dashdot$). The plot below the matrices connects the snapshot times of the matrices via the vertical $\dash\dash$. For each snapshot, we illustrate the probabilities of the $P(M_{\bullet} \rightarrow \sigma_0)$ causal direction (\bullet connected by $\textcolor{blue}{—}$), its opposing $P(M_{\bullet} \leftarrow \sigma_0)$ represented by \blacksquare connected by $\textcolor{red}{—}$, and the probability, $P(M_{\bullet} \perp \sigma_0)$, that M_{\bullet} and σ_0 are independent (\blacktriangle connected by $\textcolor{green}{\cdots\cdots}$); $P(M_{\bullet} \rightarrow \sigma_0) + P(M_{\bullet} \leftarrow \sigma_0) + P(M_{\bullet} \perp \sigma_0) = 1$. The horizontal lines at $P = 0.4$ ($\textcolor{black}{\dots\dots}$) and $P = 0.3$ ($\textcolor{black}{—}$) represent the null probabilities for the independency case and causal directional cases, respectively. Thus, significance occurs when the plotted solid lines are further away from the solid horizontal line and the plotted dotted line is significantly different from the horizontal dotted line. For example, the snapshot at $T_{\text{peak}} - 216$ Myr demonstrates a period of transition that lacks any meaningful causal information because all values are near their null values.

346 A similar fit and subsequent inversion is performed for
347 stellar mass.

348
$$\mathcal{M}^* = (10.53 \pm 0.19) + (0.31 \pm 0.01)(M_{\bullet} - 7.07)$$

349
$$\epsilon = 0.19 \pm 0.03$$

350
$$M_{\bullet} = 7.07 + \frac{\mathcal{M}^* - (10.53 \pm 0.19)}{0.31 \pm 0.01} \quad (4)$$

4.3. Elliptical (i.e., Quenched) Galaxies

351 For quenched galaxies with the correct causal direction
352 from $\sigma_0 \rightarrow M_{\bullet}$, we directly fit a relation for the
353 M_{\bullet} - σ_0 relation from the 35 elliptical galaxies in Paper I.

355
$$M_{\bullet} = (9.17 \pm 0.39) + (5.13 \pm 0.01)(S_0 - 2.44) \quad (5)$$

356
$$\epsilon = 0.38 \pm 0.05$$

357 Similarly, we can directly fit M_{\bullet} as a function of M^* .

358
$$M_{\bullet} = (9.17 \pm 0.38) + (1.37 \pm 0.00)(M^* - 11.22) \quad (6)$$

359
$$\epsilon = 0.38 \pm 0.06$$

4.4. A Correction for Spiral/Star-forming Galaxies

360 If a black hole mass were improperly fit based on
361 Equation 1, we can combine it with Equation 3 to create
362 the following equation to causally correct the black hole
363 mass.

$$\begin{aligned} 365 \quad S_0 &= A + B(M_{\bullet} - 7.07) \\ 366 \quad M'_{\bullet} &= \alpha + \beta(S_0 - 2.28) \\ 367 \quad M_{\bullet} &= 7.07 + \frac{M'_{\bullet} - \alpha - \beta(A - 2.28)}{\beta B} \\ 368 \quad &= 7.07 + \frac{M'_{\bullet} - (7.46 \pm 0.61)}{0.59 \pm 0.04} \end{aligned} \quad (7)$$

369 Here, there is a unique value where $M'_{\bullet} = M_{\bullet}$ at
370 ≈ 8.02 , below which black hole masses are over-predicted
371 and above which black hole masses are under-predicted.
372 Likewise, we can do the same for incorrect masses from
373 Equation 2 by combining with Equation 4 to create the
374 following correcting formula for black hole masses de-

375 rived from stellar masses.

$$\begin{aligned} 376 \quad M^* &= A + B(M_{\bullet} - 7.07) \\ 377 \quad M'_{\bullet} &= \alpha + \beta(M^* - 10.63) \\ 378 \quad M_{\bullet} &= 7.07 + \frac{M'_{\bullet} - \alpha - \beta(A - 10.63)}{\beta B} \\ 379 \quad &= 7.07 + \frac{M'_{\bullet} - (7.86 \pm 0.72)}{0.47 \pm 0.01} \end{aligned} \quad (8)$$

380 Here, there is a unique value where $M'_{\bullet} = M_{\bullet}$ at ≈ 8.56 ,
 381 below which black hole masses are over-predicted and
 382 above which black hole masses are under-predicted.

383 5. DISCUSSION

384 5.1. Predicting SMBH Masses

385 A causation always implies a correlation⁹, but a correlation
 386 does not always imply a causation. For the
 387 M_{\bullet} - σ_0 relation, the results of Paper I and this study
 388 indicate that M_{\bullet} is *always correlated* with σ_0 , but only
 389 in the case of quenched galaxies (i.e., elliptical galaxies)
 390 is σ_0 *predominantly a cause of* M_{\bullet} . This result is also
 391 suggested from the pure study of correlations via linear
 392 regressions. N. Sahu et al. (2019b) found that the in-
 393 trinsic scatter (ϵ) of the M_{\bullet} - σ_0 relation is significantly
 394 higher for spiral galaxies ($\epsilon = 0.67$ dex) than for ellipti-
 395 cal galaxies ($\epsilon = 0.31$ dex). Furthermore, the existence
 396 of morphologically-aware black hole mass scaling rela-
 397 tions also supports the existence of distinct evolutionary
 398 pathways for late- vs. early-type galaxies (A. W. Gra-
 399 ham & N. Scott 2013; N. Scott et al. 2013; G. Savorgnan
 400 et al. 2013; G. A. D. Savorgnan et al. 2016; B. L. Davis
 401 et al. 2018, 2019; N. Sahu et al. 2019a,b, 2020, 2022a,b;
 402 A. W. Graham & N. Sahu 2023). In a more absolute
 403 scenario, C.-H. Chen et al. (2025) present evidence for
 404 naked “little red dots” (LRDs) with essentially no de-
 405 tectable host galaxy (cf. Y. Zhang et al. 2025). Thus,
 406 black holes would be the answer to the *chicken-or-the-*
 407 *egg dilemma* of which came first, making black holes the
 408 default cause of their subsequent host galaxies (in young
 409 star-forming galaxies).

410 G. S. Novak et al. (2006) explored several black hole
 411 mass scaling relations (including the M_{\bullet} - σ_0 relation) in
 412 search of the “true” (i.e., causal) correlations of SMBHs.
 413 They emphasized that in order to arrive at the cor-
 414 rect theory governing black hole mass scaling relations,
 415 it is essential to determine the correlation with the

416 smallest intrinsic residual variance, which will have the
 417 best chance of being causally related to SMBH mass.
 418 Furthermore, G. S. Novak et al. (2006) discussed that
 419 knowledge of the direction of the causal link between
 420 SMBH mass and galactic properties is required to cor-
 421 rectly sort variables into their roles as “dependent” or
 422 “independent.” In the absence of such knowledge, it is
 423 necessary to always treat variables x and y symmetri-
 424 cally in linear regressions. Lastly, G. S. Novak et al.
 425 (2006) describe the different goals of a theorist vs. an
 426 observer; a theorist is always concerned with obtaining
 427 the causally-motivated relation (i.e., the lowest intrinsic
 428 scatter), while the observer is only interested in predict-
 429 ing black hole masses (i.e., M_{\bullet} is always the dependent
 430 variable).

431 From our results, we find that the “theorist” and the
 432 “observer” will only agree on applying the M_{\bullet} - σ_0 re-
 433 lation to elliptical galaxies. For elliptical galaxies, the
 434 intrinsic scatter will be minimized and both the theorist
 435 and the observer will use σ_0 to predict M_{\bullet} . For spiral
 436 galaxies, the theorist will prefer to use σ_0 as the depen-
 437 dent variable with M_{\bullet} as the independent variable, and
 438 the observer will probably find some other relation that
 439 minimizes the predicted error on M_{\bullet} . For the observer,
 440 obtaining more accurate M_{\bullet} estimates can be more read-
 441 ily obtained by switching or adding more variables (Z.
 442 Jin & B. L. Davis 2023; B. L. Davis & Z. Jin 2023; B.
 443 Davis & Z. Jin 2024). Overall, our method of apply-
 444 ing causal discovery provides a more definitive method
 445 of determining causal correlations beyond simply per-
 446 forming linear regressions and searching for the lowest
 447 intrinsic scatter.

488 5.2. Implications for High- z Galaxies

489 Our results concerning the causal directions in the
 490 M_{\bullet} - σ_0 relation portend the need for careful consider-
 491 ation when predicting black hole masses at high red-
 492 shifts. The peak of star formation (also known as “cos-
 493 mic noon”) occurred at $z \approx 2$ (P. Madau & M. Dickinson
 494 2014). With the *James Webb Space Telescope (JWST)*
 495 now regularly measuring the mass of SMBHs at redshifts
 496 of at least $z \approx 7$ (e.g., H. Übler et al. 2023; M. A. Stone
 497 et al. 2024; K. Inayoshi & R. Maiolino 2025), it is crucial
 498 that the methods used to measure these SMBH masses
 499 are correctly applied. Because these *JWST*-discovered
 500 SMBHs all existed well before cosmic noon (more like
 501 cosmic morning), they come from an era of the Universe
 502 that was predominantly star-forming.

503 This star-forming dependence implies that naïvely ap-
 504 plying the M_{\bullet} - σ_0 relation, and indirect methods that
 505 are calibrated to the M_{\bullet} - σ_0 relation like single-epoch
 506 spectra or reverberation mapping, to all galaxies is not

⁹ In principle, causation implies a correlation, however, the correlation may not always be detectable. Non-linear relations, countervailing causes, and dichotomous or manipulated samples may make it difficult to determine a significant correlation (specifically, linear correlation).

causally motivated. Based on our causal analysis shown in Fig. 4 and described in §3.3, we find the causal reversal of the $M_{\bullet}-\sigma_0$ relation occurs around the peak of star formation, with transitions beginning 432 Myr before T_{peak} and ending 647 Myr before $T_{z=0}$. Adapting this trend to the general population of galaxies, we estimate that this translates to $M_{\bullet} \rightarrow \sigma_0$ at $z \gtrsim 2.1$ ($\lesssim 3.1$ Gyr after the Big Bang) and $M_{\bullet} \leftarrow \sigma_0$ at $z \lesssim 0.047$ ($\lesssim 0.65$ Gyr before $T_{z=0}$).¹⁰ Thus, we find that use of the unmodified $M_{\bullet}-\sigma_0$ relation (and its derivatives) to predict black hole masses is causally-justified broadly at $z \lesssim 0.047$ (luminosity distances closer than ≈ 210 Myr). The intermediate period at $0.047 \lesssim z \lesssim 2.1$ may allow for partial justification of causally-based M_{\bullet} prediction, whereas epochs at $z \gtrsim 2.1$ are likely not causally-supported. Nonetheless, elliptical galaxies (or any types of quenched galaxies) at any redshift remain causally-motivated targets for black hole mass estimation. This long transitional period ($0.047 \lesssim z \lesssim 2.1$) lasts ≈ 10 Gyr, which is consistent with the duration of galaxies in the slow-quenching tail (i.e., taking longer than 1 Gyr to quench) that occupy a dominant fraction of the distribution (D. Walters et al. 2022).

We have demonstrated from our simulations that star-forming galaxies at high redshifts host SMBHs that are not causally beholden to stellar velocity dispersion. Therefore, we expect that there will be increased uncertainty in any SMBH mass derived from an uncorrected $M_{\bullet}-\sigma_0$ relation at high redshifts. This increased uncertainty is due to incorrectly assuming that σ_0 causes M_{\bullet} in star-forming galaxies. We expect that this excess uncertainty may be contributing to the frequent identification of so-called “overmassive” black holes at high redshifts. Notably, S. E. I. Bosman et al. (2025) show that there does not appear to be any intrinsic differences between low- z ($z < 3$) and high- z ($z > 7$) quasars, suggesting that the inferred black hole masses are possibly incorrect at both epochs.

The existence of overmassive black holes at such early epochs of the Universe has sparked intense debates concerning early black hole seeding mechanisms (M. Volonteri et al. 2023), LRDs (T. T. Ananna et al. 2024; F. M. Khan et al. 2025), obscuring interstellar media (R. Gilli et al. 2022), and super-Eddington accretion (J. Jeon et al. 2023; A. Trinca et al. 2024; H. Suh et al. 2025). Instead, we offer the simple explanation that perhaps these claims of overmassive black holes should be taken

¹⁰ Here, we specifically adopt the Planck Collaboration et al. (2020) cosmological parameters and specify cosmic noon at $z \approx 1.9$ or ≈ 3.5 Gyr after the Big Bang (P. Madau & M. Dickinson 2014).

with a grain of salt due to M_{\bullet} being causally antecedent to σ_0 , not a consequence of it in star-forming galaxies. Moreover, there are other reasons to question super-Eddington accretion and the existence of overmassive black holes in LRDs at high- z , e.g., their X-ray weakness (A. Sacchi & Á. Bogdán 2025). However, GRAVITY+ Collaboration et al. (2025) directly measured the broad-line region (BLR) dynamics of a quasar at $z = 4$; they found its derived mass “is an order of magnitude lower than that inferred from various single epoch scaling relations, and implies that that the accretion is highly super-Eddington.” Additionally, H. Übler et al. (2025, §4.1, and references therein) provide numerous explanations for why the masses of high- z are likely overestimated. Increasing doubt about the provenance of SMBHs in the early Universe will relieve the tension and need for exotic theories to explain their seemingly premature origins.

5.3. Redetermining the Masses of High- z Black Holes

For a demonstration of our causal correction to high- z black hole masses, we apply our results to the sample of 13 black holes at $4.1 < z < 10.6$ from R. Maiolino et al. (2024). R. Maiolino et al. (2024) presents a collection of star-forming, late-type systems¹¹ with black holes that are overmassive with respect to local black hole to galaxy stellar mass ratios. Their black hole masses are estimated via local single-epoch virial black hole mass relations (A. E. Reines et al. 2013; A. E. Reines & M. Volonteri 2015). However, these estimates are not directly derived from dynamical black hole masses. Instead, reverberation-mapped black hole masses are calibrated to the local $M_{\bullet}-\sigma_0$ relation, then single-epoch spectroscopic black masses are correlated with reverberation mapping via the BLR radius-luminosity relation. Therefore, single-epoch spectroscopic black hole masses are indirectly calibrated to the local $M_{\bullet}-\sigma_0$ relation.¹² Furthermore, since the local $M_{\bullet}-\sigma_0$ relation is almost exclusively fit to a sample of star-forming plus quenched galaxies, this implies that our causal correction formalism can be used to correct for the magnitude of offset in the predicted black hole masses.

Although R. Maiolino et al. (2024) do not have direct measurements of the central *stellar* velocity dispersions

¹¹ Additionally, Y. Ono et al. (2025) find that the morphological properties of high- z galaxies are statistically similar to local spiral galaxies.

¹² In this way, it is perhaps helpful to think about the connection between 1.) dynamical black hole measurements, 2.) reverberation-mapped black hole masses, and 3.) single-epoch spectroscopic black hole masses as being analogous to successive rungs on the cosmic distance ladder. If there are inaccuracies in the lowest rung of the ladder, these errors will propagate to the higher rungs of the ladder.

for their galaxies, they are able to accurately measure the velocity dispersion of *gas* from their high-resolution spectra. From there, they are able to make small corrections (R. Bezanson et al. 2018) to closely approximate the stellar velocity dispersion. The result is an effective central stellar velocity dispersion that can be used as a good proxy for the type of σ_0 that is used in local scaling relations. We use these values with our causal $M_{\bullet}-\sigma_0$ relations to estimate revised black hole masses.

In Table 2, we present the published black hole masses (M'_{\bullet}) of R. Maiolino et al. (2024) and their black hole to galaxy stellar mass ratios (M'_{\bullet}/M^*), then we present our revised causally correct black hole mass estimates (M_{\bullet}) and similarly revised black hole to galaxy stellar mass ratios (M_{\bullet}/M^*). Figure 5 illustrates the revised black hole masses on the $M_{\bullet}-\sigma_0$ diagram. The figure further shows the graphical representation of our linear regressions for the fit to all galaxy types (Equation 1), elliptical (quenched) galaxies (Equation 5), and spiral (star-forming) galaxies (Equation 3). This comparison shows a clear difference between the fits to star-forming versus quenched galaxies. Moreover, this shows that a naïve fit to all galaxies is similar to the fit for quenched galaxies, and produces overmassive black holes when applied to star-forming galaxies.

Our results show a clear decrease in the estimated black hole masses (and black hole to galaxy stellar mass ratios) for these high-redshift objects, with a median reduction of 1.93 ± 0.51 dex. This reduction effectively erases the appearance of being overmassive with high black hole to galaxy stellar mass ratios that resemble highly-evolved galaxies. For instance, the median M_{\bullet}/M^* ratios from Paper I are -2.05 ± 0.29 dex and -3.42 ± 0.44 dex for ellipticals and spirals, respectively. For comparison, the median M'_{\bullet}/M^* ratio from R. Maiolino et al. (2024) is -1.56 ± 0.74 dex versus the median M_{\bullet}/M^* ratio of -3.22 ± 0.63 dex after our reduction from causal correction (see Figure 6 for the distribution of ratios). Therefore, the ratios were previously consistent with those of highly-evolved elliptical galaxies, whereas after our causal rectification the ratios now closely match the ratios of young star-forming galaxies, which should be the case for galaxies at $4.1 < z < 10.6$ without much cosmic time to evolve. Indeed, this range of redshifts implies an age of the Universe at only 0.44–1.5 Gyr after the Big Bang (Planck Collaboration et al. 2020), leaving very little time for evolution.

5.4. Conclusions

Drawing together the threads of this investigation, we have successfully leveraged the burgeoning field of causal discovery, applied to cosmological hydrodynam-

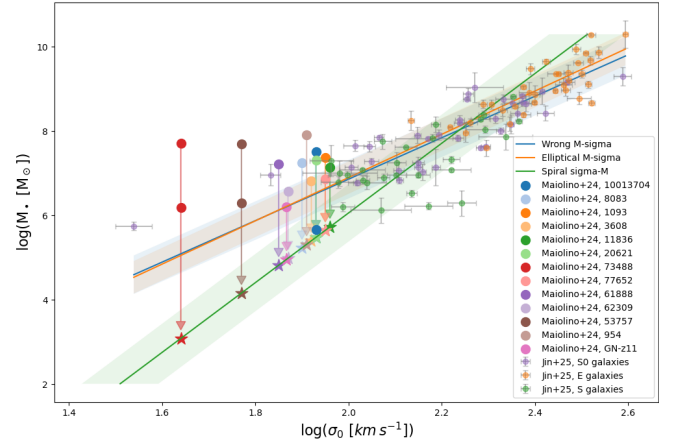


Figure 5. Linear regressions to the $z = 0$ observational data from Paper I, along with the published and revised high- z black hole masses in 13 star-forming, late-type systems from R. Maiolino et al. (2024). The 101 galaxies are divided into 38 lenticular/S0 (●), 35 elliptical/E (○), and 28 spiral/S (●) galaxies. The — line is the “wrong” fit to all 101 galaxies defined by Equation 1. The — line is the fit to the 35 elliptical (quenched) galaxies, according to the $M_{\bullet} \rightarrow \sigma_0$ causal direction, defined by Equation 5. The — line is the fit to the 28 spiral (star-forming) galaxies, according to the $\sigma_0 \rightarrow M_{\bullet}$ causal direction, defined by Equation 3. Each line is surrounded by its color’s shaded region, depicting the intrinsic scatter bounds. The larger assorted color ● points represent the published black hole masses from R. Maiolino et al. (2024) with down arrows pointing to similar-colored ★ stars, depicting our revised black hole masses. *NB:* three of the galaxies from R. Maiolino et al. (2024) have dual BLR AGNs and are depicted here with two different ● points each.

ical simulations from the NIHAO suite, to temporally resolve the causal relationship between SMBHs and their host galaxies. Our simulations not only reproduce the observed causal dichotomy between spiral and elliptical galaxies—where SMBHs appear to drive evolution in star-forming spirals but are passive participants in ellipticals—but critically, they provide robust insight into its origin. The key finding reveals a distinct causal reversal coincident with the epoch of peak star-formation, transitioning from SMBH-driven influence during active star-formation phases to a more passively correlated growth governed by hierarchical assembly in quenched systems. These results offer compelling support for theoretical models positing that AGNs feedback plays a crucial role in shaping star-forming galaxies, while subsequent growth is primarily dictated by the host galaxy’s merger and accretion history. This study underscores the immense potential of causal discovery techniques in unraveling the complex interplay governing not only SMBH and their host galaxies, but in any set of intertwined properties in other fields of as-

Table 2. 13 Revised High- z Black Hole Masses from R. Maiolino et al. (2024)

ID	Comp.	z	\mathcal{M}^*	σ_0	\mathcal{M}'_\bullet	$\mathcal{M}'_\bullet/\mathcal{M}^*$	\mathcal{M}_\bullet	$\mathcal{M}_\bullet/\mathcal{M}^*$
			[log M _⊙]	[log km/s]	[log M _⊙]	[dex]	[log M _⊙]	[dex]
(1)	(2)	(3)	(4)	(5)	(6)	(7)	(8)	(9)
10013704	BLR1	5.9	8.88 ± 0.66	$1.93^{+0.05}_{-0.06}$	5.65 ± 0.31	-3.23 ± 0.73	5.47 ± 0.83	-3.41 ± 1.06
	BLR2				7.50 ± 0.31	-1.38 ± 0.73		
8083		4.6	8.45 ± 0.03	$1.90^{+0.06}_{-0.07}$	7.25 ± 0.31	-1.20 ± 0.31	5.23 ± 0.88	-3.22 ± 0.88
1093		5.6	8.34 ± 0.20	$1.95^{+0.05}_{-0.06}$	$7.36^{+0.32}_{-0.31}$	-0.98 ± 0.37	5.64 ± 0.83	-2.70 ± 0.85
3608		5.3	$8.38^{+0.11}_{-0.15}$	$1.92^{+0.06}_{-0.07}$	$6.82^{+0.38}_{-0.33}$	-1.56 ± 0.38	5.39 ± 0.88	-2.99 ± 0.89
11836		4.4	7.79 ± 0.30	$1.96^{+0.05}_{-0.06}$	7.13 ± 0.31	-0.66 ± 0.43	5.72 ± 0.83	-2.07 ± 0.88
20621		4.7	8.06 ± 0.70	$1.93^{+0.06}_{-0.07}$	7.30 ± 0.31	-0.76 ± 0.77	5.47 ± 0.88	-2.59 ± 1.12
73488	BLR1	4.1	9.78 ± 0.20	$1.64^{+0.11}_{-0.15}$	6.18 ± 0.30	-3.60 ± 0.36	3.08 ± 1.30	-6.70 ± 1.32
	BLR2				7.71 ± 0.30	-2.07 ± 0.36		
77652		5.2	$7.87^{+0.16}_{-0.28}$	$1.95^{+0.06}_{-0.07}$	$6.86^{+0.35}_{-0.34}$	-1.01 ± 0.41	5.64 ± 0.88	-2.23 ± 0.91
61888		5.9	8.11 ± 0.92	$1.85^{+0.07}_{-0.09}$	7.22 ± 0.31	-0.89 ± 0.97	4.81 ± 0.97	-3.30 ± 1.33
62309		5.2	$8.12^{+0.12}_{-0.13}$	$1.87^{+0.07}_{-0.08}$	$6.56^{+0.32}_{-0.31}$	-1.56 ± 0.34	4.98 ± 0.94	-3.14 ± 0.94
53757	BLR1	4.4	$10.18^{+0.13}_{-0.12}$	$1.77^{+0.09}_{-0.11}$	$6.29^{+0.33}_{-0.32}$	-3.89 ± 0.35	4.15 ± 1.09	-6.03 ± 1.10
	BLR2				$7.69^{+0.32}_{-0.31}$	-2.49 ± 0.34		
954		6.8	$10.66^{+0.09}_{-0.10}$	1.91 ± 0.06	7.90 ± 0.30	-2.76 ± 0.31	5.31 ± 0.86	-5.35 ± 0.86
GN-z11		10.6	$8.90^{+0.20}_{-0.30}$...	6.20 ± 0.30	-2.70 ± 0.39	$4.95 \pm 1.16^*$	-3.95 ± 1.18

NOTE— Column (1): Galaxy identification number. Column (2): Different components for galaxies with dual BLR AGNs. Column (3): Redshift. Column (4): Galaxy stellar mass (logarithmic solar masses). Column (5): Central stellar velocity dispersion (logarithmic km/s) approximated from the gaseous stellar velocity dispersion via corrections from R. Bezanson et al. (2018). Column (6): Black hole mass (logarithmic solar masses) estimated from local virial relations (A. E. Reines et al. 2013; A. E. Reines & M. Volonteri 2015). Column (7): Black hole to galaxy stellar mass ratio (dex) according to R. Maiolino et al. (2024). Column (8): Black hole mass (logarithmic solar masses) estimated from Equation 3. Column (9): Black hole mass to galaxy stellar mass ratio (dex) according to this work.

* Derived from Equation 7.

628 trophysics (e.g., Z. Jin et al. 2025a; B. L. Davis et al.
629 2025a,b; W. Zhang et al. 2025; H. Desmond & J. Ramsey
630 2025). Finally, a causally-reversed $M_\bullet-\sigma_0$ relation
631 casts considerable doubt on the validity of SMBH mass
632 estimates for distant galaxies and challenges the pre-
633 vailing view of overmassive black holes existing in the
634 early Universe. Toward that problem, we offer a set of
635 causally-informed relations to produce black hole mass
636 estimates with improved fidelity that are consistent with
637 $z = 0$ SMBH–galaxy stellar mass ratios.

ACKNOWLEDGMENTS

639 This material is based on work supported by Tamkeen
640 under the NYU Abu Dhabi Research Institute grant
641 CASS. F.Y. is supported by the NSF of China (grants
642 12133008, 12192220, 12192223, and 12361161601). This
643 research has used NASA’s Astrophysics Data System.

644 This research was carried out on the high-performance
645 computing resources at New York University Abu
646 Dhabi.

647 *Software:* causal-learn (Y. Zheng et al. 2023),
648 Cosmology Calculator, Gym (G. Brockman et al. 2016),
649 Hyper-Fit (A. S. G. Robotham & D. Obreschkow 2015,
650 2016), JAX (J. Bradbury et al. 2018), Matplotlib (J. D.
651 Hunter 2007), NetworkX (A. A. Hagberg et al. 2008),
652 NumPy (C. R. Harris et al. 2020), Pandas (W. McKinney
653 2010), pgmpy (A. Ankan & A. Panda 2015),
654 PyGraphviz, pynbody (A. Pontzen et al. 2013), Python
655 (G. Van Rossum & F. L. Drake 2009), SciPy (P. Virtanen
656 et al. 2020), seaborn (M. L. Waskom 2021)

ORCID IDS

657 Benjamin L. Davis 

658 <https://orcid.org/0000-0002-4306-5950>

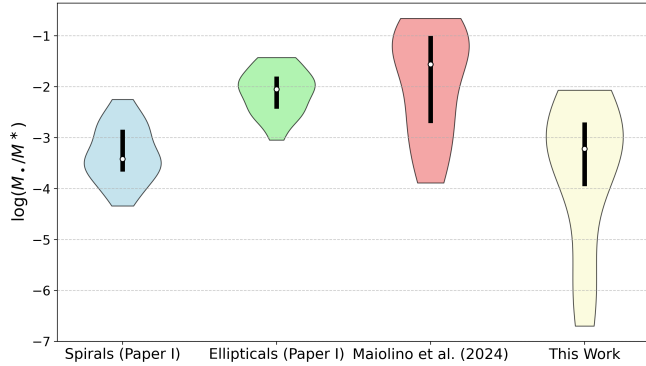


Figure 6. Violins plots showing the distribution of black hole to galaxy stellar mass ratios with indicators for their medians and the interquartile ranges. Moving from left to right: we show the sample of spiral galaxies from Paper I with a median of -3.42 ± 0.44 dex, the elliptical galaxies from Paper I with a median of -2.05 ± 0.29 dex, the high- z late-type galaxies with black hole masses estimated by R. Maiolino et al. (2024) with a median of -1.56 ± 0.74 dex, and the same high- z late-type galaxies with black hole masses re-determined via our causally-informed correction (Equation 3) with a median of -3.22 ± 0.63 dex.

REFERENCES

- 668 Ananna, T. T., Bogdán, Á., Kovács, O. E., Natarajan, P., & Hickox, R. C. 2024, *ApJL*, 969, L18
 669
 670 Ankan, A., & Panda, A. 2015, in Proceedings of the 14th Python in Science Conference (SCIPY 2015), Citeseer
 671
 672 Bezanson, R., van der Wel, A., Straatman, C., et al. 2018, *ApJL*, 868, L36
 673
 674 Blank, M., Macciò, A. V., Dutton, A. A., & Obreja, A. 2019, *MNRAS*, 487, 5476
 675
 676 Bosman, S. E. I., Álvarez-Márquez, J., Davies, F. B., et al. 2025, *arXiv e-prints*, arXiv:2511.02902
 677
 678 Bradbury, J., Frostig, R., Hawkins, P., et al. 2018,, 0.3.13 <http://github.com/google/jax>
 679
 680 Brockman, G., Cheung, V., Pettersson, L., et al. 2016, *arXiv e-prints*, arXiv:1606.01540
 681
 682 Chen, C.-H., Ho, L. C., Li, R., & Zhuang, M.-Y. 2025, *ApJ*, 983, 60
 683
 684 Ciotti, L., & Ostriker, J. P. 1997, *ApJL*, 487, L105
 685
 686 Ciotti, L., & van Albada, T. S. 2001, *ApJL*, 552, L13
 687 Davis, B., & Jin, Z. 2024, in American Astronomical Society Meeting Abstracts, Vol. 56, American Astronomical Society Meeting Abstracts, 152.06
 688
 689 Davis, B. L., Ali-Dib, M., Zheng, Y., et al. 2025a, *arXiv e-prints*, arXiv:2507.03760
 690
 691 —. 2025b, *MNRAS*, 543, L34
 692 Davis, B. L., Graham, A. W., & Cameron, E. 2018, *ApJ*, 869, 113
 693
 694 —. 2019, *ApJ*, 873, 85
 695 Davis, B. L., & Jin, Z. 2023, *ApJL*, 956, L22
 696 Desmond, H., & Ramsey, J. 2025, *arXiv e-prints*, arXiv:2510.01112
 697
 698 Fabian, A. C. 2012, *ARA&A*, 50, 455
 699 Ferrarese, L., & Merritt, D. 2000, *ApJL*, 539, L9
 700 Gebhardt, K., Bender, R., Bower, G., et al. 2000, *ApJL*, 539, L13
 701
 702 Gilli, R., Norman, C., Calura, F., et al. 2022, *A&A*, 666, A17
 703
 704 Graham, A. W., & Sahu, N. 2023, *MNRAS*, 518, 2177
 705
 706 Graham, A. W., & Scott, N. 2013, *ApJ*, 764, 151
 707 GRAVITY+ Collaboration, El Dayem, K. A., Aimar, N., et al. 2025, *arXiv e-prints*, arXiv:2509.13911
 708 Hagberg, A. A., Schult, D. A., & Swart, P. J. 2008, in
 709 Proceedings of the 7th Python in Science Conference, ed.
 710 G. Varoquaux, T. Vaught, & J. Millman, Pasadena, CA
 711 USA, 11 – 15
 712 Harris, C. R., Millman, K. J., van der Walt, S. J., et al.
 713 2020, *Nature*, 585, 357–362
 714 Harrison, C. M., & Ramos Almeida, C. 2024, *Galaxies*, 12,
 715 17
 716 Huber, M. 2024, *arXiv e-prints*, arXiv:2407.08602
 717 Hunter, J. D. 2007, *Computing in Science & Engineering*, 9,
 718 90–95
 719 Ikeuchi, S. 1999, *Advances in Space Research*, 23, 865
 720 Inayoshi, K., & Maiolino, R. 2025, *ApJL*, 980, L27

- 721 Jeon, J., Liu, B., Bromm, V., & Finkelstein, S. L. 2023,
 722 *MNRAS*, 524, 176
- 723 Jin, Z., & Davis, B. L. 2023, *arXiv e-prints*,
 724 arXiv:2310.19406
- 725 Jin, Z., Lu, Y., Ting, Y.-S., Zheng, Y., & Buck, T. 2025a,
 726 *arXiv e-prints*, arXiv:2507.00134
- 727 Jin, Z., Pasquato, M., Davis, B., Maccio, A., & Hezaveh, Y.
 728 2025b, in American Astronomical Society Meeting
 729 Abstracts, Vol. 245, American Astronomical Society
 730 Meeting Abstracts #245, 120.03D
- 731 Jin, Z., Pasquato, M., Davis, B. L., Macciò, A. V., &
 732 Hezaveh, Y. 2024, *arXiv e-prints*, arXiv:2410.14775
- 733 Jin, Z., Pasquato, M., Davis, B. L., et al. 2025c, *ApJ*, 979,
 734 212
- 735 Jorgensen, I., Franx, M., & Kjaergaard, P. 1995, *MNRAS*,
 736 276, 1341
- 737 Khan, F. M., Davis, B. L., Macciò, A. V., &
 738 Holley-Bockelmann, K. 2025, *ApJL*, 986, L1
- 739 Kormendy, J., & Ho, L. C. 2013, *ARA&A*, 51, 511
- 740 Madau, P., & Dickinson, M. 2014, *ARA&A*, 52, 415
- 741 Maiolino, R., Scholtz, J., Curtis-Lake, E., et al. 2024, *A&A*,
 742 691, A145
- 743 Makarov, D., Prugniel, P., Terekhova, N., Courtois, H., &
 744 Vauglin, I. 2014, *A&A*, 570, A13
- 745 Mastichiadis, A., & Kirk, J. G. 1995, in International
 746 Cosmic Ray Conference, Vol. 2, International Cosmic
 747 Ray Conference, 33
- 748 McKinney, W. 2010, in Proceedings of the 9th Python in
 749 Science Conference, Vol. 445, Austin, TX, 51–56
- 750 Morganti, R. 2017, *Frontiers in Astronomy and Space
 751 Sciences*, 4, 42
- 752 Novak, G. S., Faber, S. M., & Dekel, A. 2006, *ApJ*, 637, 96
- 753 Ono, Y., Ouchi, M., Harikane, Y., et al. 2025, *ApJ*, 991, 222
- 754 Pasquato, M. 2024, in EAS2024, European Astronomical
 755 Society Annual Meeting, 362
- 756 Pasquato, M., Jin, Z., Lemos, P., Davis, B. L., & Macciò,
 757 A. V. 2023, *arXiv e-prints*, arXiv:2311.15160
- 758 Pearl, J. 2000, Causality (Cambridge University Press)
- 759 Planck Collaboration, Aghanim, N., Akrami, Y., et al.
 760 2020, *A&A*, 641, A6
- 761 Pontzen, A., Roškar, R., Stinson, G., & Woods, R. 2013,,
 762 Astrophysics Source Code Library, record ascl:1305.002
- 763 Reines, A. E., Greene, J. E., & Geha, M. 2013, *ApJ*, 775,
 764 116
- 765 Reines, A. E., & Volonteri, M. 2015, *ApJ*, 813, 82
- 766 Renzini, A. 2000, in Exploring the Universe, ed. H. Gursky,
 767 R. Ruffini, & L. Stella, 229–241
- 768 Robotham, A. S. G., & Obreschkow, D. 2015, *PASA*, 32,
 769 e033
- 770 Robotham, A. S. G., & Obreschkow, D. 2016,, *Astrophysics*
 771 Source Code Library, record ascl:1601.002
- 772 Sacchi, A., & Bogdán, Á. 2025, *ApJL*, 989, L30
- 773 Sahu, N., Graham, A. W., & Davis, B. L. 2019a, *ApJ*, 876,
 774 155
- 775 —. 2019b, *ApJ*, 887, 10
- 776 —. 2020, *ApJ*, 903, 97
- 777 —. 2022a, *Acta Astrophysica Taurica*, 3, 39
- 778 —. 2022b, *ApJ*, 927, 67
- 779 Savorgnan, G., Graham, A. W., Marconi, A., et al. 2013,
 780 *MNRAS*, 434, 387
- 781 Savorgnan, G. A. D., Graham, A. W., Marconi, A., & Sani,
 782 E. 2016, *ApJ*, 817, 21
- 783 Schawinski, K., Thomas, D., Sarzi, M., et al. 2007,
 784 *MNRAS*, 382, 1415
- 785 Scott, N., Graham, A. W., & Schombert, J. 2013, *ApJ*, 768,
 786 76
- 787 Silk, J., & Rees, M. J. 1998, *A&A*, 331, L1
- 788 Springel, V., White, S. D. M., Jenkins, A., et al. 2005,
 789 *Nature*, 435, 629
- 790 Stone, M. A., Lyu, J., Rieke, G. H., Alberts, S., & Hainline,
 791 K. N. 2024, *ApJ*, 964, 90
- 792 Suh, H., Scharwächter, J., Farina, E. P., et al. 2025, *Nature
 793 Astronomy*, 9, 271
- 794 Tremaine, S., Gebhardt, K., Bender, R., et al. 2002, *ApJ*,
 795 574, 740
- 796 Trinca, A., Valiante, R., Schneider, R., et al. 2024, *arXiv
 797 e-prints*, arXiv:2412.14248
- 798 Übler, H., Maiolino, R., Curtis-Lake, E., et al. 2023, *A&A*,
 799 677, A145
- 800 Übler, H., Mazzolari, G., Maiolino, R., et al. 2025, *arXiv
 801 e-prints*, arXiv:2509.21575
- 802 Van Rossum, G., & Drake, F. L. 2009, Python 3 Reference
 803 Manual (Scotts Valley, CA: CreateSpace)
- 804 Virtanen, P., Gommers, R., Oliphant, T. E., et al. 2020,
 805 *Nature Methods*, 17, 261
- 806 Volonteri, M., Habouzit, M., & Colpi, M. 2023, *MNRAS*,
 807 521, 241
- 808 Wadsley, J. W., Keller, B. W., & Quinn, T. R. 2017,
 809 *MNRAS*, 471, 2357
- 810 Walters, D., Woo, J., & Ellison, S. L. 2022, *MNRAS*, 511,
 811 6126
- 812 Wang, L., Dutton, A. A., Stinson, G. S., et al. 2015,
 813 *MNRAS*, 454, 83
- 814 Wang, T., Xu, K., Wu, Y., et al. 2024, *Nature*, 632, 1009
- 815 Waskom, M. L. 2021, *Journal of Open Source Software*, 6,
 816 3021
- 817 Wyithe, J. S. B., & Loeb, A. 2003, *ApJ*, 595, 614
- 818 Zanga, A., Ozkirimli, E., & Stella, F. 2023, *arXiv e-prints*,
 819 arXiv:2305.10032

- 820 Zhang, W., Lin, Q., Ting, Y.-S., et al. 2025, arXiv e-prints,
821 arXiv:2509.23901
822 Zhang, Y., Ding, X., Yang, L., et al. 2025, arXiv e-prints,
823 arXiv:2510.25830
824 Zheng, Y., Huang, B., Chen, W., et al. 2023, arXiv e-prints,
825 arXiv:2307.16405